

Effect of dipolar interactions on cavity magnon polaritons

Antoine Morin , Christian Lacroix , and David Ménard

Department of Engineering Physics, Polytechnique Montréal, Montréal, Québec, Canada H3T 1J4



(Received 14 September 2020; accepted 2 December 2020; published 18 December 2020)

The strong photon-magnon coupling between an electromagnetic cavity and two yttrium iron garnet (YIG) spheres has been investigated in the context of a strong mutual dipolar interaction between the spheres. A decrease in the coupling strength between the YIG spheres and the electromagnetic cavity is observed, along with an increase of the total magnetic losses, as the distance between the spheres is decreased. A model of inhomogeneous broadening of the ferromagnetic resonance linewidth, partly mitigated by the dipolar narrowing effect, reproduces the reduction in the coupling strength observed experimentally. These findings have important implications for the understanding of a strongly coupled photon-magnon system involving densely packed magnetic objects, such as ferromagnetic nanowire arrays, in which the total coupling strength with an electromagnetic cavity might become limited due to mutual dipolar interactions.

DOI: [10.1103/PhysRevB.102.224421](https://doi.org/10.1103/PhysRevB.102.224421)

I. INTRODUCTION

Following recent works on the strong coupling between a magnonic mode of a ferromagnetic sample and a photonic mode of a microwave cavity [1,2], also called cavity magnon polaritons [3,4], much interest emerged in the scientific community to exploit the phenomenon as a mean to develop novel information transfer technologies [5–10]. Some interesting propositions involve multiple yttrium iron garnet (YIG) spheres placed inside an electromagnetic cavity, such as the magnon gradient memory [11], the long distance modification of spin currents [12], and the development of ultrahigh sensitivity magnetometers [13].

As these new ideas are being elaborated [14], it is important to correctly predict the behavior of photon-magnon systems consisting of several ferromagnetic elements coupled to an electromagnetic resonator. In this context, the effect of dipolar interactions between the ferromagnetic objects on the strong photon-magnon coupling is crucial and remains relatively unexplored.

The strong coupling of photon-magnon systems is well understood and has been recently reviewed [15]. Its extension to multiple independent magnons is relatively straightforward [16]. For an ensemble of N independent and identical ferromagnetic objects, the ideal coupling is expected to be enhanced by a factor of \sqrt{N} as compared to the coupling strength of a single object to the cavity. However, due to dipolar interactions between the magnetic elements, some detuning along with inhomogeneous broadening are expected for coupled magnon systems. In this paper, we investigate the coupling strength of a simplified system consisting of two YIG spheres coupled to an adjustable microwave cavity. We show experimentally that the coupling constant g decreases as the spheres are brought closer. The results are explained using a model based on the Landau-Lifshitz equation and the Fourier expansion of the magnetization in order to include the coupling of the photons with the uniform ferromagnetic mode as well as with the long wavelength spin wave modes,

which are excited in the presence of a nonuniform magnetic field.

II. EXPERIMENTAL PROCEDURE

A tunable waveguide cavity consisting of a shorted X-band waveguide in which a metallic rod of 1.36 mm of diameter is inserted in a slit located on one side of the waveguide [17] was used, as shown in Fig. 1. Varying the position of the rod along the slit and its length inside the waveguide allowed the tuning of the volume, resonance frequency, and electromagnetic losses of the cavity. For the experiments, the TE_{109} mode with $\omega_c/2\pi = 11.69$ GHz (volume $V_c = 32.37$ cm³) was chosen [18]. The cavity and the YIG spheres were excited by a vector network analyzer, which was also used as a detector to obtain the resonance spectra for different applied fields through the S_{11} reflection coefficient. In order to observe the strong coupling regime, the spheres were placed on the shorted end of the waveguide resonator where the amplitude of the rf magnetic field is maximum. The two spheres, which will be called YIG₁ and YIG₂ hereafter, have a radius $R_1 = 0.62 \pm 0.01$ mm and $R_2 = 0.61 \pm 0.01$ mm, respectively. They were placed so that the center line (or axis) generated by the two spheres was parallel to the direction of the external DC magnetic field H_0 . The center-to-center distance d of the spheres was varied from 1.41 to 3.58 mm.

The strong coupling regime is observed when the coupling constant g exceeds both the cavity losses κ_c and the magnetic losses κ_m [6]. This is illustrated in Fig. 2 for YIG₁, where the hybridization of the cavity photonic mode and the ferromagnetic uniform mode of resonance is observed. In this work, the rod insertion was adjusted to have κ_c comparable to κ_m in order to facilitate the observation of the coupling. The coupling g is obtained by subtracting the resonance frequency of both modes for the whole range of magnetic fields, whereas the minimum value is equal to $2g$. The value of the magnetic field corresponding to this minimum will be called H_c .

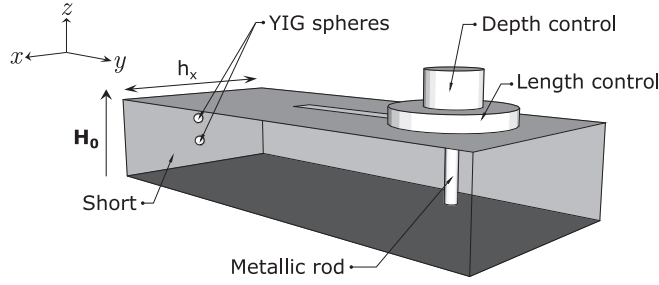


FIG. 1. Schematic representation of the tunable cavity used experimentally. The metallic rod allows the tuning of the resonance frequency and the losses of the cavity. The direction of the field H_0 and the rf magnetic field h_x are also shown.

III. RESULTS

A coupling constant of $g_1/2\pi = 29.2$ MHz and $g_2/2\pi = 28.5$ MHz was independently extracted for YIG₁ and YIG₂, respectively. This agrees well with the theoretical value given by [5]

$$g = \eta \sqrt{\frac{V_s}{V_c}} \left(\frac{\omega_M \omega_c}{2} \right)^{1/2}, \quad (1)$$

where V_s is the volume of the sphere, $\omega_M = \mu_0 |\gamma| M_s$ with M_s the saturation magnetization, γ the gyromagnetic ratio, and η represents the spatial overlap between the cavity photonic mode and the magnonic mode. The factor η is given by [19]

$$\eta = \left| \frac{1}{h_{\max} m_{\max} V_s} \int_{\text{sphere}} (\mathbf{h} \cdot \mathbf{m}) dV \right|, \quad (2)$$

where \mathbf{h} is the dynamic magnetic field of the cavity with h_{\max} being its maximum magnitude and \mathbf{m} is the dynamic magnetization of the sphere with m_{\max} being its maximum magnitude. The value of η is usually equal to 1 when \mathbf{h} and \mathbf{m} are both uniform, which is the case for a small sample placed at the maximum of the cavity field.

The input-output formalism [6] was used to extract the losses of each component. The losses of the cavity $\kappa_c/2\pi$ were ≈ 8.65 MHz, similar to the losses $\kappa_{m1}/2\pi = 8.44$ MHz

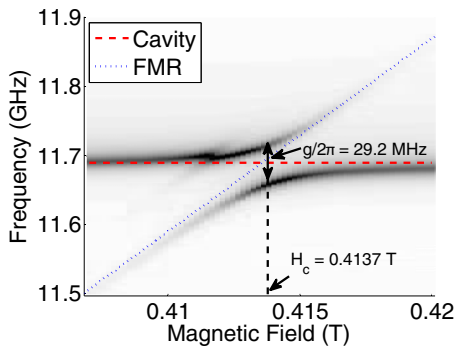


FIG. 2. Strong coupling spectra obtained for the sphere YIG₁ with the setup described in Sec. II. The extracted coupling constant is $g_1/2\pi = 29.2$ MHz. The hybridization of the modes occurs at a field $H_c = 0.4137$ T. When there is no coupling, the resonance frequency of the cavity and the YIG sphere is represented by the red dashed line and the blue dotted line, respectively.

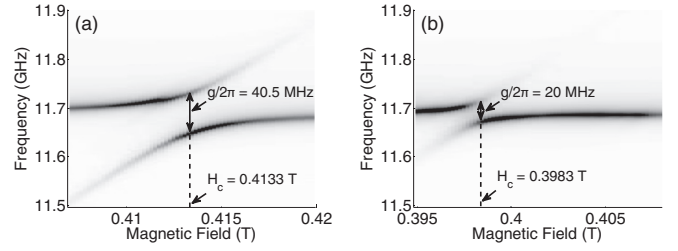


FIG. 3. Strong coupling between the microwave cavity and two YIG spheres placed at a mutual distance of (a) $d = 3.58$ mm and (b) $d = 1.41$ mm. The dipolar interaction between the spheres shifts the value of H_c and decreases the total coupling constant g .

(YIG₁) and $\kappa_{m2}/2\pi = 12.63$ MHz (YIG₂) of the YIG spheres. The mean magnetic losses of both spheres, equal to 10.54 MHz, will be referred to as $\bar{\kappa}_{m\infty}$ hereafter.

With two spheres in the cavity, the hybridization of the modes is still exhibited, but accompanied with a shift in the value of H_c and a change in the coupling strength as the spheres are brought closer. This is shown in Fig. 3 for two values of d . Knowing that the dipolar field of a uniformly polarized sphere is rigorously equivalent to that of its equivalent point dipole [20], the field shift, due to the dipolar interaction, can be calculated by solving the coupled Landau-Lifshitz equations of motion of the two spheres treated as macrospins:

$$\frac{\partial}{\partial t} \begin{bmatrix} \mathbf{M}_1 \\ \mathbf{M}_2 \end{bmatrix} = -\mu_0 |\gamma| \begin{bmatrix} \mathbf{M}_1 \\ \mathbf{M}_2 \end{bmatrix} \times \left(\mathbf{H} + \bar{\mathbf{N}} \begin{bmatrix} \mathbf{M}_2 \\ \mathbf{M}_1 \end{bmatrix} \right), \quad (3)$$

where

$$\bar{\mathbf{N}} = \frac{1}{3} \left(\frac{R}{d} \right)^3 \begin{bmatrix} -1 & 0 & 0 \\ 0 & -1 & 0 \\ 0 & 0 & 2 \end{bmatrix}, \quad (4)$$

$\mathbf{H} = H_0 \hat{z} + \mathbf{h}$, R is the mean radius of the spheres, considered identical, and d is the distance between the macrospins. Using a small signal approximation, the coupled equations yield the resonance condition

$$\omega_{\text{res}} = \omega_0 + \left(\frac{R}{d} \right)^3 \omega_M, \quad (5)$$

where $\omega_0 = \mu_0 |\gamma| H_0$. Because the hybridization of the modes occurs for $\omega_{\text{res}} = \omega_c$, Eq. (5) shows that smaller distances d lead to smaller values of H_c . This shift of H_c was used to corroborate and correct the distances between the spheres, which were initially measured manually with a digital micrometer. A good agreement has been found between the two methods. The field shift could be more accurately calculated by considering the nonuniformity of the dipolar field over the volume of the spheres, but this additional contribution was calculated to be negligible.

The reduction of the coupling constant g , exhibited in Fig. 3 as the spheres are brought closer, is reported in greater detail in Fig. 4 (closed circles). For large distances between the spheres, one expects from the input-output formalism [21] a total coupling strength of approximately $\sqrt{g_1^2 + g_2^2}$ (dotted line), which is indeed observed. However, for smaller distances d , the coupling constant is observed to decrease sharply from 40.5 MHz down to 20 MHz.

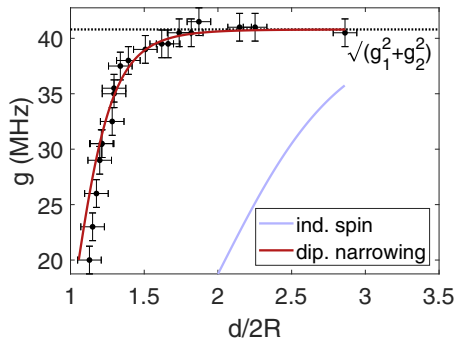


FIG. 4. Effect of dipolar interactions on the total coupling strength g obtained experimentally (closed circles). Pale-blue curve: Expected decrease in the case of independent spins calculated with Eq. (8). Dark-red curve: Expected decrease in the case of dipolar narrowing calculated with Eq. (12). Dotted line: Coupling constant when $d \rightarrow \infty$.

Considering the two YIG spheres as a whole, the usual expression of the S_{11} reflection coefficient, calculated from the input-output formalism, was used to extract the magnetic losses of the two spheres as a function of the distance between the spheres $\bar{\kappa}_m(d)$ (closed circles in Fig. 5). In contrast with g , the magnetic losses increase sharply as the spheres get closer. For a distance $d = 1.41$ mm ($d/2R = 1.13$), the magnetic losses are just above 16 MHz, which is near the coupling strength of 20 MHz. For shorter distances, the magnetic losses would continue to increase while the coupling constant would decrease, causing the system to exit the strong coupling regime.

IV. DISCUSSION

In order to explain the reduction of the coupling constant, let us consider the impact of the dipolar interaction on η . The dipolar field can be separated into two components. A dominant nonuniform static component is added to the applied static field and tends to spread the local field on the spheres. A weaker nonuniform dynamic field is further added to the

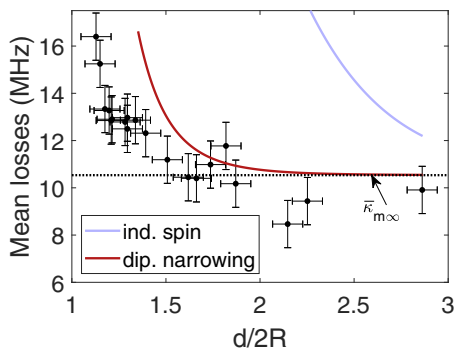


FIG. 5. Magnetic losses $\bar{\kappa}_m$ obtained experimentally as the spheres get closer (closed circles). Pale-blue curve: Expected increase in linewidth when considering independent spins extracted from the susceptibility calculated with Eq. (8). Dark-red curve: $\bar{\kappa}_{m\infty} + \Delta\omega$ where $\Delta\omega$ is calculated using Eq. (11). Dotted line: Magnetic losses when $d \rightarrow \infty$.

cavity pumping field, which could result in the excitation of nonuniform resonance modes. Assuming that the rf magnetic field of the unperturbed cavity is uniform, we can rewrite η in terms of the uniform mode susceptibility using $\mathbf{m} = \chi\mathbf{h}$. Since the real part of the susceptibility $\chi' \approx 0$ near resonance, we keep only the imaginary part and rewrite Eq. (2) as

$$\eta = \frac{1}{\chi''_{\max} V_s} \int_{\text{sphere}} \chi'' dV = \frac{\langle \chi'' \rangle}{\chi''_{\max}}, \quad (6)$$

where the brackets $\langle \cdot \rangle$ represent the mean value over the volume of the sphere.

Further insights are provided by examining two limiting cases. Case 1 corresponds to the macrospin approximation, in which all spins in a sphere are strongly coupled and locked parallel to each other's, which was assumed earlier in Eq. (3). Our calculations indicate that the dynamic part of both spheres will be in phase, resulting in a constant factor $\eta = 1$ for any distance d . In Fig. 4, the macrospin approximation corresponds to the dotted line and a value of $g = \sqrt{g_1^2 + g_2^2}$. Likewise, the macrospin approximation does not lead to an increase in the linewidth observed in Fig. 5 but rather gives a constant linewidth of $\bar{\kappa}_{m\infty}$ (dotted line).

In contrast, case 2 assumes fully independent spins, that is, no long-range dynamic dipolar interaction and each spin constituent of the spheres is resonating at its own frequency depending on the value of its local static magnetic field. This nonuniform magnetic field, assumed to be along the $\hat{\mathbf{z}}$ direction, is given by $H_z = H_0 + H_{\text{dip.}}$, where

$$H_{\text{dip.}} = \frac{R^3[r^2(3\cos^2\vartheta - 1) + 4dr\cos\vartheta + 2d^2]}{3(r^2 + 2dr\cos\vartheta + d^2)^{5/2}} M_s. \quad (7)$$

Here, $H_{\text{dip.}}$ is the static dipolar magnetic field and the variables r and ϑ determine the position in a spherical coordinates system centered on a sphere placed at a distance d from the source dipole. One can then numerically compute the probability density function $f(H_{\text{dip.}})$ over the volume of the sphere as a function of d to calculate the value of the mean susceptibility of the independent spins ensemble at resonance ($\omega = \omega_c$). Assuming no magnetic anisotropy, we have

$$\langle \chi'' \rangle = \int_{H_z} \frac{\bar{\kappa}_{m\infty} \omega M}{(\mu_0 |\gamma| |H_z - \omega_c|^2 + \bar{\kappa}_{m\infty}^2)} f(H_z) dH_z, \quad (8)$$

which can be substituted in (6) and then (1) to calculate the coupling. In this limiting case, a strong decrease in η is predicted, even for spheres separated by a relatively large distance d , as shown by the pale blue curve in Fig. 4. Furthermore, the inhomogeneously broadened linewidth in the independent spins approximation is given by the pale-blue line in Fig. 5, which predicts a much broader linewidth than observed experimentally.

In our two spheres experiment, we thus fall somewhere between these two limits: macrospin and independent spins. A more rigorous approach should include long-range dynamic dipolar interactions which are known to produce a phenomenon called ‘‘dipolar narrowing’’ in the literature [22]. We consider the original approach used by Clogston [23] in which the Landau-Lifshitz equation of motion is solved for a nonuniform magnetic field expanded in Fourier components

as

$$H_z = \sum_{\mathbf{k}} H_{\mathbf{k}} e^{i\mathbf{k}\cdot\mathbf{r}}. \quad (9)$$

Assuming that the field inhomogeneity is low with respect to the sample dimensions, we can neglect the terms related to the exchange interaction in the equation of motion, but consider the terms associated with dynamic dipolar fields. Further expanding the magnetization in Fourier series and by following a procedure similar to Ref. [23], we can derive an analytical expression for the imaginary part of the susceptibility of the uniform mode of resonance, accounting for the coupling between the uniform mode and the long-wavelength spin wave modes, a process called two-magnon scattering [24]. With some simplifications, it can be written in the form

$$\langle \chi'' \rangle = \frac{(\bar{\kappa}_{m\infty} + \Delta\omega)\omega_M}{(\omega - \omega_c)^2 + (\bar{\kappa}_{m\infty} + \Delta\omega)^2}, \quad (10)$$

where

$$\Delta\omega = \frac{\pi}{2} \frac{\text{Var}(\omega_{\text{dip.}})}{\omega_M} \left[1 + \frac{1}{2} \left(\frac{\omega_M}{3\omega_c - \omega_M} \right) \right]^2 \times \left[\frac{2}{3} - \left(\frac{\omega_c}{3\omega_c - \omega_M} \right) \right]^{-1/2} \quad (11)$$

is an additional loss term directly related to the variance of the static dipolar magnetic field through the quantity $\omega_{\text{dip.}} = \mu_0 |\gamma| |H_{\text{dip.}}|$, which can be calculated analytically (see Appendix). In the expression of $\Delta\omega$, the division by ω_M represents the dipolar narrowing effect. This additional loss term is added to $\bar{\kappa}_{m\infty}$, which yields a total loss term that can be compared with the measured mean losses of the magnetic system. As shown by the dark-red curve in Fig. 5, the general trend of the data is reproduced relatively well.

Regarding the coupling constant g , the definition of η in Eq. (6) is extended to account for the fact that spins, whose resonance frequency $\mu_0 |\gamma| |H_z|$ is detuned from the resonance frequency of the cavity ω_c , can contribute to the coupling with the cavity. This can be achieved by introducing a weight function in the definition of η so that the spins whose resonance frequency is contained inside the coupling range ($\pm g$ around ω_c), have a stronger contribution (high energy exchange) to the total coupling than those whose resonance frequency falls outside the coupling range (low energy exchange). In contrast, in Eq. (6), only the spins resonating at frequency ω_c contribute, whereas the remaining spins (detuned from the cavity) do not contribute to the coupling. To include this phenomenon, we use a weight function consisting in a Lorentz distribution $\mathcal{L}(\omega_c, g_{\text{max}})$ centered at $\omega = \omega_c$ and having a half-width at half maximum of $g_{\text{max}} = \sqrt{g_1^2 + g_2^2}$. We thus have

$$\eta = \frac{\int_0^\infty \frac{(\bar{\kappa}_{m\infty} + \Delta\omega)\omega_M \mathcal{L}(\omega_c, g_{\text{max}})}{(\omega - \omega_c)^2 + (\bar{\kappa}_{m\infty} + \Delta\omega)^2} d\omega}{\int_0^\infty \frac{\bar{\kappa}_{m\infty}\omega_M \mathcal{L}(\omega_c, g_{\text{max}})}{(\omega - \omega_c)^2 + \bar{\kappa}_{m\infty}^2} d\omega}, \quad (12)$$

which equals unity if $\Delta\omega = 0$, in absence of dipolar broadening. Equation (12) may be used with Eq. (1) to generate the dark-red curve in Fig. 4. The excellent agreement with the experimental data supports that the observed decrease in the coupling rate between the system of magnetic spheres and the cavity, as the spheres are brought closer together,

originates from the increasingly nonuniform dipolar static magnetic field on each sphere. It also shows that the long-range dynamic dipolar interaction within each sphere, which gives rise to the dipolar narrowing effect, somewhat limits the adverse effect of the nonuniform field distribution.

Similarly, the expression of η given in (12) implies that a larger coupling g_{max} tends to smooth out the adverse effect of a given dipolar broadening $\Delta\omega$ in reducing the total coupling strength. For the shortest distances between the spheres ($d/2R < 1.18$), the model seems to systematically predict a higher coupling constant for a fixed distance than what is experimentally observed. This could be due to the underlying assumptions made in the model, providing possible paths for improvement.

V. CONCLUSION

We have demonstrated that the dipolar interaction between two ferromagnetic objects can strongly affect their coupling with a microwave cavity. As the distance between the spheres is gradually reduced, dipolar interactions force the spins to resonate at increasingly different frequencies. This results in increased magnetic losses and decreased coupling strength g of the system. A model based on inhomogeneous broadening with dipolar narrowing reproduces the main features observed on a system consisting of two YIG spheres in a tunable microwave cavity. While the reduction in the coupling strength can be linked with the variance of applied field caused by the dipolar interaction, this effect is attenuated by dipolar narrowing and by strong coupling of each individual sphere with the cavity.

Our results suggest that a number of N individual ferromagnetic objects inserted in an electromagnetic cavity will eventually exhibit a reduced coupling as compared to the expected $g \propto \sqrt{N}$ behavior as the density is increased. Yet the dipolar broadening will be mitigated by a compensating dipolar narrowing effect. A trade-off must be found to determine the optimal density of ferromagnetic objects to be placed in the cavity to reach a maximum coupling strength while reducing the impact of dipolar interaction.

APPENDIX: ANALYTICAL EXPRESSION FOR $\text{Var}(\omega_{\text{dip.}})$

Integrating by parts Eq. (7), we have

$$\langle \omega_{\text{dip.}} \rangle = \frac{a^3}{12} \omega_M, \quad (A1)$$

where $a = 2R/d$ ($0 \leq a \leq 1$). The integration by parts also leads to an analytical expression for $\langle \omega_{\text{dip.}}^2 \rangle$. The definition of the variance, $\text{Var}(\omega_{\text{dip.}}) = \langle \omega_{\text{dip.}}^2 \rangle - \langle \omega_{\text{dip.}} \rangle^2$, then gives

$$\frac{\text{Var}(\omega_{\text{dip.}})}{\omega_M^2} = \frac{a^3}{4} \left\{ \frac{a}{3(4-a^2)^3} \left[5 + \frac{a^2}{2} \left(1 + \frac{a^2}{8} \right) \right] + \frac{\tanh^{-1}(a/2)}{24} - \frac{a}{4} \left(\frac{3}{32} + \frac{a^2}{9} \right) - \frac{3(4-a^2)}{512} \ln \left(\frac{2+a}{2-a} \right) \right\}. \quad (A2)$$

- [1] Ö. O. Soykal and M. E. Flatté, Strong Field Interactions between a Nanomagnet and a Photonic Cavity, *Phys. Rev. Lett.* **104**, 077202 (2010).
- [2] H. Huebl, C. W. Zollitsch, J. Lotze, F. Hocke, M. Greifenstein, A. Marx, R. Gross, and S. T. B. Goennenwein, High Cooperativity in Coupled Microwave Resonator Ferrimagnetic Insulator Hybrids, *Phys. Rev. Lett.* **111**, 127003 (2013).
- [3] Y. Cao, P. Yan, H. Huebl, S. T. B. Goennenwein, and G. E. W. Bauer, Exchange magnon-polaritons in microwave cavities, *Phys. Rev. B* **91**, 094423 (2015).
- [4] B. M. Yao, Y. S. Gui, Y. Xiao, H. Guo, X. S. Chen, W. Lu, C. L. Chien, and C.-M. Hu, Theory and experiment on cavity magnon-polariton in the one-dimensional configuration, *Phys. Rev. B* **92**, 184407 (2015).
- [5] Y. Tabuchi, S. Ishino, T. Ishikawa, R. Yamazaki, K. Usami, and Y. Nakamura, Hybridizing Ferromagnetic Magnons and Microwave Photons in the Quantum Limit, *Phys. Rev. Lett.* **113**, 083603 (2014).
- [6] X. Zhang, C.-L. Zou, L. Jiang, and H. X. Tang, Strongly Coupled Magnons and Cavity Microwave Photons, *Phys. Rev. Lett.* **113**, 156401 (2014).
- [7] P. Hyde, L. Bai, M. Harder, C. Dyck, and C.-M. Hu, Linking magnon-cavity strong coupling to magnon-polaritons through effective permeability, *Phys. Rev. B* **95**, 094416 (2017).
- [8] M. Goryachev, W. G. Farr, D. L. Creedon, Y. Fan, M. Kostylev, and M. E. Tobar, High-cooperativity cavity qed with magnons at microwave frequencies, *Phys. Rev. Appl.* **2**, 054002 (2014).
- [9] Y. Tabuchi, S. Ishino, A. Noguchi, T. Ishikawa, R. Yamazaki, K. Usami, and Y. Nakamura, Coherent coupling between a ferromagnetic magnon and a superconducting qubit, *Science* **349**, 405 (2015).
- [10] N. J. Lambert, J. A. Haigh, S. Langenfeld, A. C. Doherty, and A. J. Ferguson, Cavity-mediated coherent coupling of magnetic moments, *Phys. Rev. A* **93**, 021803(R) (2016).
- [11] X. Zhang, C.-L. Zou, N. Zhu, F. Marquardt, L. Jiang, and H. X. Tang, Magnon dark modes and gradient memory, *Nat. Commun.* **6**, 8914 (2015).
- [12] L. Bai, M. Harder, P. Hyde, Z. Zhang, C.-M. Hu, Y. P. Chen, and J. Q. Xiao, Cavity Mediated Manipulation of Distant Spin Currents Using a Cavity-Magnon-Polariton, *Phys. Rev. Lett.* **118**, 217201 (2017).
- [13] Y. Cao and P. Yan, Exceptional magnetic sensitivity of \mathcal{PT} -symmetric cavity magnon polaritons, *Phys. Rev. B* **99**, 214415 (2019).
- [14] J. T. Hou and L. Liu, Strong Coupling between Microwave Photons and Nanomagnet Magnons, *Phys. Rev. Lett.* **123**, 107702 (2019).
- [15] M. Harder and C.-M. Hu, Cavity spintronics: An early review of recent progress in the study of magnon-photon level repulsion, in *Solid State Physics* (Elsevier, New York, 2018), Vol. 69, pp. 47–121.
- [16] D. Zhang, X.-M. Wang, T.-F. Li, X.-Q. Luo, W. Wu, F. Nori, and J. You, Cavity quantum electrodynamics with ferromagnetic magnons in a small yttrium-iron-garnet sphere, *npj Quantum Inf.* **1**, 1 (2015).
- [17] A. Morin, C. Lacroix, and D. Ménard, Strong coupling of electromagnetic and magnetic modes in a tunable waveguide cavity, in *2016 17th International Symposium on Antenna Technology and Applied Electromagnetics (ANTEM)* (IEEE, New York, 2016), pp. 1–2.
- [18] D. M. Pozar, *Microwave engineering* (Wiley, New York, 2009).
- [19] N. Lambert, J. Haigh, and A. Ferguson, Identification of spin wave modes in yttrium iron garnet strongly coupled to a coaxial cavity, *J. Appl. Phys.* **117**, 053910 (2015).
- [20] B. F. Edwards, D. M. Riffe, J.-Y. Ji, and W. A. Booth, Interactions between uniformly magnetized spheres, *Am. J. Phys.* **85**, 130 (2017).
- [21] D. I. Schuster, A. P. Sears, E. Ginossar, L. DiCarlo, L. Frunzio, J. J. L. Morton, H. Wu, G. A. D. Briggs, B. B. Buckley, D. D. Awschalom, and R. J. Schoelkopf, High-Cooperativity Coupling of Electron-Spin Ensembles to Superconducting Cavities, *Phys. Rev. Lett.* **105**, 140501 (2010).
- [22] S. M. Rezende and A. Azevedo, Dipolar narrowing of ferromagnetic resonance lines, *Phys. Rev. B* **44**, 7062 (1991).
- [23] A. Clogston, Inhomogeneous broadening of magnetic resonance lines, *J. Appl. Phys.* **29**, 334 (1958).
- [24] R. D. McMichael, D. J. Twisselmann, and A. Kunz, Localized Ferromagnetic Resonance in Inhomogeneous Thin Films, *Phys. Rev. Lett.* **90**, 227601 (2003).